DOI: 10.1002/ejic.200800140

Infrared Spectra of Insertion, Methylidene, and Methylidyne Complexes in Reactions of Laser-Ablated Ruthenium Atoms with Halomethanes and Methane

Han-Gook Cho[a] and Lester Andrews*[b]

Keywords: Ruthenium complexes / Matrix isolation / Infrared spectra / Density functional calculations

Reactions of laser-ablated Ru atoms with halomethanes and methane have been investigated. Small carbyne and carbene complexes or insertion products are produced in the reactions of halomethanes via C–X insertion and halogen migration, whereas only the insertion complex is formed in the reactions of methane. The results are consistent with computed product stabilities. The diagnostic C–H and C–X stretching absorptions of the carbyne complexes are observed on the blue side of the corresponding precursor bands. The high C–H and C–X stretching frequencies are explained with the higher s character in hybridization and combination with the C≡Ru stretching motion, respectively. The structures of the carbyne complexes are highly distorted and show a large variation with the ligands, and the extra electron pair on the Ru atom evidently plays an important role in the carbyne. In contrast to early transition-metal analogs, the Ru carbene complexes show no agostic distortion.

Introduction

The importance of transition metal complexes with a carbon–metal multiple bond has increased continuously since their discovery in the 1970s.[1,2] Recently transition-metal complexes containing the carbyne moiety have received considerable attention for their bonding properties as well as their growing applications in various syntheses, particularly alkyne metathesis.[3] Among the numerous carbyne complexes provided through a variety of synthetic routes, a relatively small number of Ru carbynes have been introduced in comparison with those of Mo, W, and Re complexes.[1,4,5]

Carbyne complexes containing the simple M≡C–H or M≡C–X moiety (M = transition metal) are not common.[6] In addition, the weak but important methylidyne C–H stretching bands are normally covered by other much stronger absorptions in this frequency region. As a result, the carbyne C–H and C–X vibrational characteristics remain largely uninvestigated except for the simple MCH transient species[7,8] and the H–C≡W ligand complexes.[9,10]

More recently methylidyne complexes have been prepared in reactions of laser-ablated Mo, W, Re, and Os atoms with small alkanes and halomethanes.[10–12] The methylidyne C–H stretching absorptions are observed at approximately 200 cm^{-1} above the corresponding precursor absorption and a trend of increasing frequency with the s character in the C–H bond is observed.[10–12] The low symmetry structures of Re carbynes[12a] are traced to the Jahn–Teller effect[13] in the simple complexes. The halogenated derivatives, such as ClC≡$ReCl_3$ and FC≡$ReCl_3$, show exceptionally high C–X stretching frequencies.[12] Similar low symmetry structures are also observed from small Os complexes.[11c]

The activation of C–H bonds is important in organometallic chemistry.[14] Recently C–H activation by laser-ablated transition-metal atoms has been employed to provide small carbene and carbyne complexes, many of which show unique structures and reversible photochemistry.[15] Here, we report the IR spectra of isotopic products from reactions of laser-ablated Ru atoms with halomethanes and methane. The insertion, carbene, and carbyne products are identified depending on the system, and the elusive methylidyne C–H stretching absorptions are also observed from the hydrogen-containing carbynes. Computations reveal unique structures for the products, and the structural effects of the extra electron pair on Ru are investigated.

Computational Methods

In order to support the assignment of new experimental frequencies, density functional theory (DFT) calculations were carried out using the Gaussian 03 package,[16] B3LYP density functional,[17] 6-311++G(3df,3pd) basis sets for C, H, F, Cl[18] and SDD pseudopotential and basis set[19] for

[a] Department of Chemistry, University of Incheon,
177 Dohwa-dong, Nam-ku, Incheon, 402-749, South Korea
[b] Department of Chemistry, University of Virginia,
P. O. Box 400319, Charlottesville, Virginia 22904-4319
E-mail: lsa@virginia.edu

Supporting information for this article is available on the WWW under http://www.eurjic.org or from the author.

Ru to provide a consistent set of vibrational frequencies for the reaction products. Geometries were fully relaxed during optimization, and the optimized geometry was confirmed by vibrational analysis. Several BPW91[20] calculations were also done to complement the B3LYP results. The vibrational frequencies were calculated analytically, and the zero-point energy is included in the calculation of the binding energies. Previous investigations have shown the DFT calculated harmonic frequencies are usually slightly higher than the observed frequencies,[15,21,22] depending on the mode anharmonicity, and they provide useful predictions for infrared spectra of new molecules.

Results and Discussion

Reactions of ruthenium with halomethane and methane isotopomers were carried out, and the matrix infrared spectra of new products will be compared with frequencies calculated by the density functional theory.

Ru + CF_4

Figure 1 illustrates the CF_4 spectra in the C–F and Ru–F stretching regions. The observed frequencies of the new absorptions are listed in Table 1. The product absorptions marked **m** (for methylidene) increase about 5 and 10% on visible ($\lambda > 420$ nm) and UV ($240 < \lambda < 380$ nm) irradiations, respectively. They increase another 10% on full arc ($\lambda > 220$ nm) irradiation and sharpen up in the early stage of annealing. The previous studies on reactions of metal atoms and halomethanes show that insertion, carbene, and carbyne complexes are the most probable products.[15] In this case the carbene product is the most stable: the carbene complex [CF_2=RuF_2(T)] is 56 kcal/mol more stable than the reactants while the insertion and carbyne products, CF_3–RuF(T) and FC≡RuF_3(T), are 35 and 31 kcal/mol, respectively, more stable than reactants at the B3LYP level of theory.

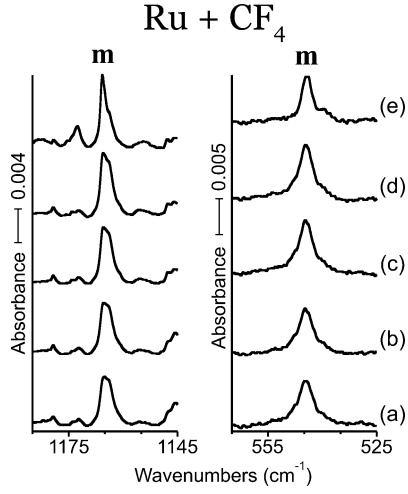

Figure 1. IR spectra in the regions of 1185–1145 and 565–525 cm^{-1} for laser-ablated Ru atoms co-deposited with CF_4 in excess argon at 8 K and their variation. (a) Lu + 0.5% CF_4 in Ar co-deposited for 1 h. (b) As (a) after photolysis ($\lambda > 420$ nm). (c) As (b) after photolysis ($240 < \lambda < 380$ nm). (d) As (c) after photolysis ($\lambda > 220$ nm). (e) As (d) after annealing to 28 K; **m** denotes the product absorption.

Moreover the observed **m** absorptions correlate with the predicted vibrational characteristics for the carbene complex (CF_2=RuF_2), which are listed in Table S1 (see Supporting Information). The observed **m** absorptions at 1165.5, 629.8 (not shown), and 544.7 cm^{-1} are assigned to the CF_2 *anti*-symmetric stretching and RuF_2 *anti*-symmetric and symmetric stretching modes of CF_2=RuF_2 as shown in Table 1. The strongest symmetric CF_2 stretching absorption is unfortunately covered by the precursor C–F stretching band. The predicted vibrational characteristics for the in-

Table 1. Frequencies of product absorptions observed from reactions of Ru and CX_4 molrcules in excess argon.[a].

	CF_4	CF_3Cl	$^{13}CF_3Cl$	CF_2Cl_2	$CFCl_3$	CCl_4	$^{13}CCl_4$	Description
m	covered[b]	1263.6, CF_2=RuFCl	1226.4, $^{13}CF_2$=RuFCl	1206.1, CF_2=$RuCl_2$ 1174.9, CFCl=RuFCl	1184.7, $RuCl_2$=CFCl	957.9, CCl_2=$RuCl_2$	920.9, $^{13}CCl_2$=$RuCl_2$	CX_2 sym. str.
	1165.5, CF_2=RuF_2		1142.6, $^{13}CF_2$=RuFCl	covered[b]	908.7, $RuCl_2$=CFCl	covered[b]	covered[b]	CX_2 asym. str.
						683.6, CCl_2=$RuCl_2$	663.3, $^{13}CCl_2$=$RuCl_2$	CX_2 wag
	629.8, CF_2=RuF_2	609.1, CF_2=RuFCl	608.3, $^{13}CF_2$=RuFCl	covered[b]				RuX_2 asym. str.
	544.7, CF_2=RuF_2			610.3, CFCl=RuFCl				RuX_2 sym. str.
y		1621.3, FC≡RuF_2Cl	1572.7, $^{13}CF_2$=RuFCl	1618.8, FC≡$RuFCl_2$ 1258.4, ClC≡RuF_2Cl	1615.0, FC≡$RuCl_3$ 1320.2, ClC≡$RuFCl_2$	1318.8, ClC≡$RuCl_3$	1272.7, $Cl^{13}C$≡$RuCl_3$	C–X str.
				590.5, FC≡$RuFCl_2$	598.1, ClC≡$RuFCl_2$			RuX_3 as. str.

[a] All frequencies are in cm^{-1}. Description gives major coordinate. [b] Covered by precursor absorption.

sertion and carbyne (Table S2) complexes do not match with the observed **m** absorptions. For example, the insertion complex would show two equally strong absorptions at around 1100 cm^{-1} about 60 cm^{-1} apart, which are not observed. The other vibrational bands of CF_2=RuF_2 are too weak to be observed (Table S1). Satisfactory agreement between the observed and predicted vibrational characteristics substantiates formation of the small carbene tetra-halide, via C–F insertion and following α-F migration during deposition and photolysis afterward. The primary formation of CF_2=RuF_2 also suggests that the α-F migration after C–F insertion is swift enough that no measurable amount of the higher energy insertion complex remains and a second α-F transfer to form the higher energy carbyne does not happen under these conditions.

Ru + CF_3Cl

We find CF_3Cl to be more reactive than CF_4, and a sharp new band at 1621.3 cm^{-1} labeled **y** (for methylidyne) in Figure 2 increases dramatically on sequential irradiation. It is significant that the carbon-13 counterpart is observed at 1572.7 cm^{-1}. A stronger band at 1263.6 cm^{-1} labeled **m** (for methylidene) increases about two-fold on irradiation and shifts to 1226.4 cm^{-1} with carbon-13 substitution and has a weaker 1142.6 cm^{-1} associated band. The carbon-13 shifts (3.0%) facilitate C–F stretching mode descriptions as a C–Cl stretch would have a relatively higher shift (3.5% compared to 3.0%, see Table S2, Supporting Information). Assignment to the very strong C–F stretching mode in FC≡RuF_2Cl follows even though the B3LYP calculation is lower than the observed by 3.6% instead of the other way around. In earlier work we find the C–F stretching frequency in methylidyne complexes to be high in the appropriate region.[12] The strongest C–F stretching mode in CF_2=RuFCl is predicted at 1275.1 cm^{-1} and the observed **m** band is in excellent agreement (Table S1). The 1142.6 cm^{-1} band is due to the weaker C–F stretching mode that is obscured in the carbon-12 compound, and the 609.1 cm^{-1} band is ascribed to the Ru–F stretching mode.

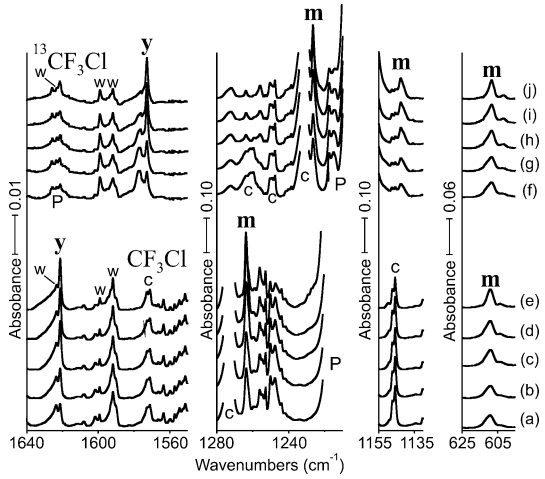

Figure 2. IR spectra in selected regions of 1640–1550, 1280–1210, 1155–1130, and 625–595 cm^{-1} for laser-ablated Ru atoms co-deposited with CF_3Cl in excess argon at 8 K and their variation. (a) Ru + 0.5% CF_3Cl in Ar co-deposited for 1 h. (b) As (a) after photolysis ($\lambda > 420$ nm). (c) As (b) after photolysis ($240 < \lambda < 380$ nm). (d) As (c) after photolysis ($\lambda > 220$ nm). (e) As (d) after annealing to 28 K. (f) Ru + 0.5% $^{13}CF_3Cl$ (90% enriched) in Ar co-deposited for 1 h. (g) As (f) after photolysis ($\lambda > 420$ nm). (h) As (g) after photolysis ($240 < \lambda < 380$ nm). (i) As (h) after photolysis ($\lambda > 220$ nm). (j) As (i) after annealing to 28 K; **m** and **y** denote the product absorption group.

Shown in Figure 3 are the CF_2Cl_2 spectra in the C–F, C–Cl, and Ru–F stretching regions. Due to the presence of the two different halogen atoms in the precursor, more than one structural isomer is possible for each reaction product. The **m** absorptions at 1206.1 cm^{-1} in the C–F stretching region remains unchanged on visible photolysis and increases about 7% on UV photolysis. It increases another 7% on full arc photolysis and decreases fast on annealing. On the other hand the **m′** absorptions at 1174.9 and 610.3 cm^{-1} increase 5 and 20% on visible and UV photolysis, respectively. They also increase 15% on full arc photolysis. The absorptions of possible CF_2Cl_2 fragments (e.g., CF_2, CFCl, and CCl_2) are not observed. [23–25]

Ru + CF_2Cl_2

Similar to the Ru + CF_4 system, DFT calculations show that the insertion complexes are less stable relative to the carbene and carbyne complexes; $CFCl_2$–RuF(Q) and CF_2Cl–RuCl(Q) are 44 and 58 kcal/mol lower in energy than the reactants, whereas CF_2=$RuCl_2$(T), CFCl=RuFCl-(T), and CCl_2=RuF_2 are 99, 84, and 73 kcal/mol lower, and FC≡$RuFCl_2$(T) and ClC≡RuF_2Cl(T) are 75 and 67 kcal/mol lower in energy than the reactants.

The strong **m** and **m′** C–F stretching bands around 1200 cm^{-1} suggest that they originate from carbene products with C–F bonds. We assign the **m** absorption at 1206.1 cm^{-1} to the symmetric CF_2 stretching mode of CF_2=$RuCl_2$ on the basis of correlation with the predicted value (1271 cm^{-1} frequency from Table S1).[21,22] However, the antisymmetric stretching band predicted at 1124 cm^{-1}, the other observably strong absorption from CF_2=$RuCl_2$, is unfortunately overlapped by a precursor absorption. The **m′** absorptions at 1174.9 and 610.3 cm^{-1} are assigned to the C–F and Ru–F stretching modes of CFCl=RuFCl on the basis of a reasonable agreement with the predicted values. The C–Cl stretching absorption is covered by a strong precursor band. All other bands of CF_2=$RuCl_2$ and CFCl=RuFCl in our instrumental range are too weak to be observed.

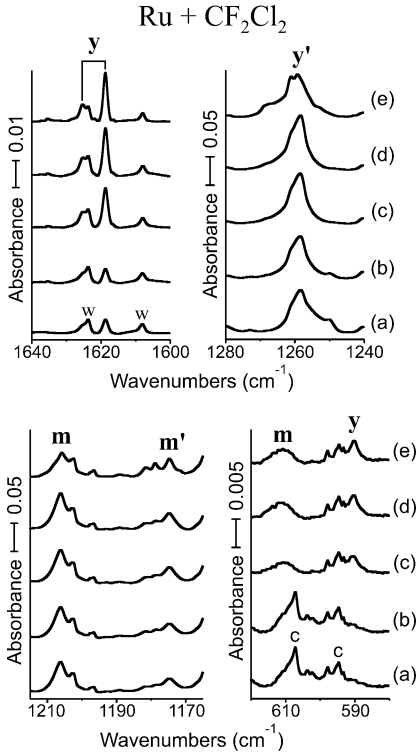

Figure 3. IR spectra in the regions of 1640–1600, 1280–1240, 1215–1165, and 620–580 cm^{-1} for laser-ablated Ru atoms co-deposited with CF_2Cl_2 in excess argon at 8 K and their variation. (a) Ru + 0.5% CF_2Cl_2 in Ar co-deposited for 1 h. (b) As (a) after photolysis ($\lambda > 420$ nm). (c) As (b) after photolysis ($240 < \lambda < 380$ nm). (d) As (c) after photolysis ($\lambda > 220$ nm). (e) As (d) after annealing to 28 K; **m**, **m′**, **y**, and **y′** denote the product absorption group.

The **y** product absorptions at 1625.2, 1618.8, and 590.5 cm^{-1} remain unchanged on visible photolysis but triple on UV photolysis and increase slightly more on full arc photolysis. On the other hand, the **y′** absorption at 1258.4 cm^{-1} increases about 30 and 10% on UV and full arc photolysis, respectively. We designate the **y** absorptions at 1625.2 and 1618.8 cm^{-1} (split by the matrix) to the C–F stretching mode of $FC{\equiv}RuFCl_2$ on the basis of the exceptionally high C–F stretching frequencies,[12] and the one at 590.5 cm^{-1} to the Ru–F stretching mode. The other absorptions of $FC{\equiv}RuFCl_2$ are predicted too weak to be observed (Table S2, Supporting Information). The initially weak **y** absorptions and dramatic increases on photolysis afterward indicate that the formation of $FC{\equiv}RuFCl_2$ is less favored during deposition, but it is initiated by photolysis.

The **y′** product absorption at 1258.4 cm^{-1} is on the other hand assigned to the C–Cl stretching mode of $ClC{\equiv}RuF_2Cl$. The carbyne C–Cl stretching frequency is also unusually high in comparison with the precursor C–Cl stretching frequencies and the most C–Cl stretching bands appearing in the region of 785–540 cm^{-1}. The remarkably high C–F and C–Cl stretching frequencies of the carbyne complexes are due to coupled C–X and C–Ru stretching motions. Mode analyses describe the high "C–X stretching mode" as the antisymmetric X–C–Ru stretching mode. The present results also show that $ClC{\equiv}RuF_2Cl$, which is predicted 8 kcal/mol higher energy than $FC{\equiv}RuFCl_2$, is primarily formed in the reaction of the laser ablated/excited Ru atoms with CF_2Cl_2 during co-deposition, suggesting that F migration is faster relative to the Cl migration under the conditions of these experiments.

$$Ru + CF_2Cl_2 \rightarrow CFCl_2{-}RuF^* \rightarrow CCl_2{=}RuF_2^* \rightarrow ClC{\equiv}RuF_2Cl$$

In the following photolysis, however, the lower energy $FC{\equiv}RuFCl_2$ isomer is produced much faster (the absorptions triple) on UV photolysis than $ClC{\equiv}RuF_2Cl$, whose absorption barely increases. The present results also show that parallel to Cr, Mo, W,[15] Re, and Os,[11,12] Ru forms carbyne complexes in reaction with tetrahalomethanes.

Ru + $CFCl_3$

Figure 4 shows the $CFCl_3$ spectra in the C–F, C–Cl, and Ru–F stretching regions. Two sets of product absorptions marked "**m**" and "**y**" are observed on the basis of the behaviors on photolysis (**m** and **y** for methylidene and methylidyne). Calculations show that the insertion complex is expected far less stable than the carbene and carbyne complexes; $CFCl_2$–RuCl and CCl_3–RuF are 63.4 and 51.0 kcal/mol lower in energy than the reactants.

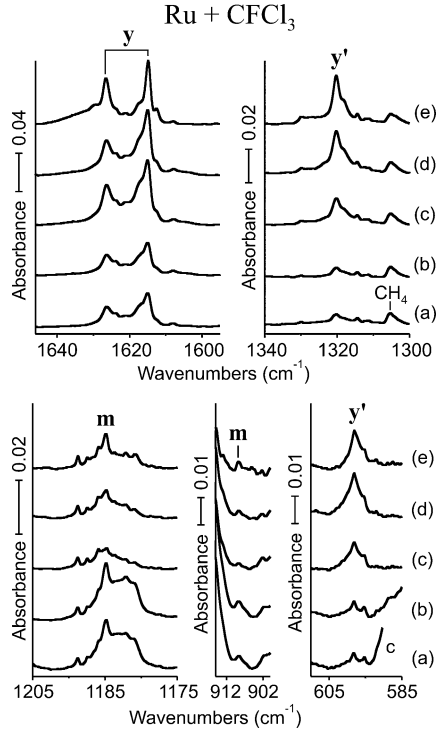

Figure 4. IR spectra in the regions of 1645–1595, 1340–1300, 1205–1175, 915–900, and 610–585 cm^{-1} for laser-ablated Ru atoms co-deposited with $CFCl_3$ in excess argon at 8 K and their variation. (a) Ru + 0.5% $CFCl_3$ in Ar co-deposited for 1 h. (b) As (a) after photolysis ($\lambda > 420$ nm). (c) As (b) after photolysis ($240 < \lambda < 380$ nm). (d) As (c) after photolysis ($\lambda > 220$ nm); **m**, **y**, and **y′** denote the product absorption groups.

The **m** product absorptions increase about 20% on visible photolysis, but dramatically decrease on UV irradiation. They partly recover on the subsequent visible photolysis and increase slightly further in the early stage of annealing. The product's C–F stretching absorption at 1184.7 cm^{-1} suggests formation of a methylidene product with a C–F bond, and we assign the **m** absorptions at 1184.7 and 908.7 cm^{-1} to the C–F and C–Cl stretching modes of $CFCl{=}RuCl_2$. $CFCl{=}RuCl_2$ is 105 kcal/mol lower in energy than the reactants. $CCl_2{=}RuFCl$, another plausible carbene product, is 92 kcal/mol lower and is not identified in the product spectra.

The two **y** absorptions at 1626.4 and 1615.0 cm^{-1} (split by the matrix) slightly decrease on visible photolysis but double on UV photolysis. They again slightly decrease on full arc photolysis and sharpen up at the early stage of annealing. The two **y′** absorptions, on the other hand, are observed at 1320.2 and 598.1 cm^{-1}. They remain unchanged on visible photolysis, but more than triple on UV photolysis and increase another 200% on full arc irradiation (quintuple in total). The unusually high C–F stretching and C–Cl stretching frequencies of the **y** and **y′** absorptions signify formation of carbyne products. We assign the **y** absorptions at 1626.4 and 1615.0 cm^{-1} to the C–F stretching mode of $FC{\equiv}RuCl_3$ and the **y′** absorptions at 1320.2 and 598.1 cm^{-1} to the C–Cl and Ru–F stretching modes of $ClC{\equiv}RuFCl_2$. The carbyne isomers $FC{\equiv}RuCl_3$ and $ClC{\equiv}RuFCl_2$ are 96 and 88 kcal/mol lower energy, respectively, than the reactants.

Ru + CCl_4

Shown in Figure 5 are the CCl_4 and $^{13}CCl_4$ spectra in the C–Cl stretching regions. The CCl_4 spectra are fairly simple. The relatively weak **m** absorption at 683.6 cm^{-1} has its ^{13}C counterpart at 663.3 cm^{-1}. Another **m** absorption is observed at 957.9 cm^{-1} in a congested area with precursor bands, and its ^{13}C counterpart at 920.9 cm^{-1} (both not shown). The insertion product [CCl_3–RuCl(Q)], which is 69 kcal/mol lower than the reactants, is expected far less stable than the carbene and carbyne complexes, which are 111 and 108 kcal/mol lower than the reactants. Moreover, CCl_3–RuCl would show two strong absorptions near 650 cm^{-1}, which are not observed in this study. The predicted vibrational characteristics of the carbyne complex (Table S2) also do not match with the **m** absorptions. We assign the **m** absorptions at 957.9 and 683.6 cm^{-1} to symmetric and *anti*-symmetric CCl_2 stretching modes of $CCl_2{=}RuCl_2$ (Table S1). This reasonable correlation between calculated and observed frequencies[21,22] supports the formation of $CH_2{=}RuCl_2$.

A very strong product absorption marked "**y**" is observed at 1318.8 cm^{-1} and its ^{13}C counterpart at 1272.7 cm^{-1} with 46.1 cm^{-1} shift. The high frequency C–Cl stretching absorption signifies formation of the carbyne product, $ClC{\equiv}RuCl_3$. Table S2 shows that the strong C–Cl stretching band is predicted at 1276.9 cm^{-1} with ^{13}C shift of 45.3 cm^{-1}. Our calculation predicts a 2.2 cm^{-1} chlorine 35 to 37 shift, which is manifest as an unresolved shoulder in the spectra of Figure 5. Parallel to the CF_2Cl_2 and $CFCl_3$ cases, the B3LYP frequency for the carbyne C–Cl stretching mode is very close to the observed values. Table S2 also shows that the other bands are expected too weak to be observed in our observation range.

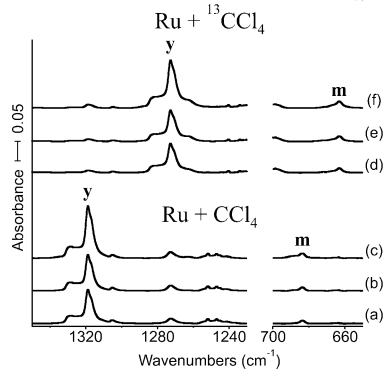

Figure 5. IR spectra in the regions of 1350–1230 and 700–650 cm^{-1} for laser-ablated Ru atoms co-deposited with CCl_4 and $^{13}CCl_4$ in excess argon at 8 K and their variations. (a) Ru + 0.5% CCl_4 in Ar co-deposited for 1 h. (b) As (a) after photolysis ($\lambda > 420$ nm). (c) As (b) after photolysis ($240 < \lambda < 380$ nm). (d) Ru + 0.5% $^{13}CCl_4$ in Ar co-deposited for 1 h. (e) As (d) after photolysis ($\lambda > 420$ nm). (f) As (e) after photolysis ($240 < \lambda < 380$ nm); **m** and **y** denote the product absorption groups.

The present results reveal that all the tetrahalomethanes produce the carbynes and/or with the carbenes in reaction with Ru atoms, while the higher energy insertion products are not identified. This is traced to the higher energy of the insertion complex relative to the higher oxidation-state complexes. Evidently the carbyne product is favored with more chlorine atoms (less fluorine atoms) in reactions of mixed halogenated methane, due to the increasing stability of the carbyne product relative to the insertion and carbene products.

However, the carbynes are predicted less stable than the carbenes even in the CCl_4 system, where the carbyne complex is the primary product. The C–Ru bond is more polarized in a higher oxidation-state complex. For example, the Mulliken charges of the carbon and ruthenium atoms in CCl_3–RuCl, $CCl_2{=}RuCl_2$, and $ClC{\equiv}RuCl_3$ are –0.53 and 1.76, –0.58 and 2.47, and –0.76 and 2.80, respectively. Because a more polarized bond is most likely stabilized more by the matrix, a higher oxidation-state complex is expected to be favored. Moreover, a higher oxidation-state complex has more Ru–X bonds, which are more polarized than the C–X bonds. Therefore, the actual energy of a carbyne product could well be lower in the matrix than those of other products, which in turn leads to the major formation of that product in tetrahalomethane systems.

Structures of Tetrahalomethane Products

Figure 6 shows the predicted structures of tetrahalocarbenes in their ground triplet states, where $CCl_2{=}RuCl_2$,

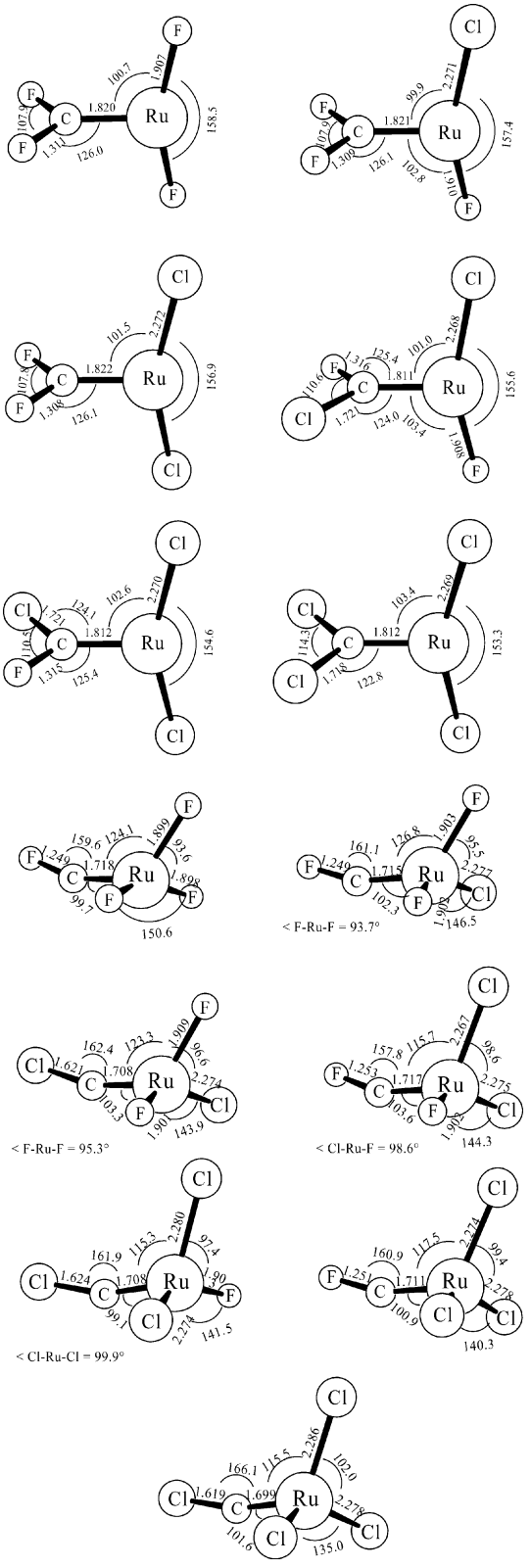

Figure 6. Optimized molecular structures of small Ru methylidene and methylidyne tetra-halide complex in the ground electronic states. The structures are calculated with B3LYP/6-311++G(3df,3pd) and the SDD core potential and basis set are used for Ru. CF_2=RuF_2, CF_2=$RuCl_2$, and CCl_2=$RuCl_2$ have a C_{2v} structure, and CFCl=$RuCl_2$ has a C_s structure. FC≡RuF_3, FC≡$RuCl_3$, and ClC≡$RuCl_3$ have C_s structures and the others have a C_1 structure. The bond lengths and angles are in Å and degrees.

CF_2=$RuCl_2$, and CF_2=RuF_2 have C_{2v} structures. These allene-type structures may be compared to the agostic, near planar structures of most small methylidenes identified from reactions of early transition metals with methane and methyl halides.[15] The absence of agostic distortion reveals the importance of the ligand effects on the carbene structure: no agostic structure was computed for small doubly or more highly halogenated small methylidenes.[26] The metal center electronic structure is also important as CH_2=RuH_2 is also calculated to be symmetrical.[27]

The carbene C=Ru bond lengths of 1.812–1.820 Å (Figure 5) are compared with those of 1.796(3) and 1.839(3) Å measured for $(H_2IMes)(PCy_3)Cl_2Ru(=C=C=CPh_2)$ and $[Ru(CH–p\text{-}C_6H_4Cl)(PCy_3)_2Cl_2]$.[28] The C=Ru and Ru–Cl bonds shorten with more chlorine atoms in the carbene structure. The lower electronegativity of chlorine relative to that of fluorine is expected to allow more electron density in the C=Ru and Ru–Cl bonds, which strengthens these bonds in the carbene complexes.

Figure 6 also illustrates the optimized structures of the small carbyne tetrahalides. The carbyne C≡Ru bond lengths of 1.699–1.718 Å are compared with that of 1.7178(16) measured for $[Ru(CPh)(O\text{-}p\text{-}C_6H_4\text{-}t\text{Bu})(PCy_3)_2]$.[28] The carbynes as well as the corresponding carbenes prepared from tetrahalomethanes all have triplet ground states. The low symmetries of the carbynes are perhaps surprising. FC≡RuF_3, FC≡$RuCl_3$, and ClC≡$RuCl_3$ have C_s structure, and the carbynes with mixed halogen atoms all have a C_1 structure. The most distorted is the structure of FC≡RuF_3, where F–C–Ru angle is 159° and one of the F atoms bonded to Ru is inclined much more than the other two (angle F–Ru–F 93.6° vs. 150.6°). The C_1 structures of ClC≡RuF_2Cl, FC≡$RuFCl_2$, and ClC≡$RuFCl_2$ are also interesting. The two Ru–F bonds in ClC≡RuF_2Cl as well as the two Ru–Cl bonds in the other two are not the same.

Figure 7 shows the HOMOs of the CH_2=RuF_2, CCl_2=$RuCl_2$, FC≡RuF_3, ClC≡RuF_2Cl, ClC≡$RuFCl_2$, and ClC≡$RuCl_3$. The extra electron pair on Ru evidently plays an important role in the structure of the carbyne complex. Notice the nodal planes between the halogen atoms. The lone electron pair on Ru provides *anti*-bonding character between the two halogen atoms bonded to the Ru atom in the carbene complex, pushing them apart (angle X–Ru–X 180°). Similarly the halogen atoms bonded to the carbon atom are also push away each other and from the halogen atoms bonded to the Ru atom, eventually forming an allene-type structure.

Likewise, two halogen atoms among the three bonded to the Ru atom in the carbyne complexes are pushed away from each other due to the extra electron pair on Ru, lowering the symmetry ϕ(FRuCF), ϕ(ClRuCF), ϕ(ClRuCF), ϕ(FRuCCl), ϕ(ClRuCCl), and ϕ(ClRuCCl) are 157.8, 150.8, 151.6, 149.0, 146.5, and 141.2°, respectively. It is also interesting that the stronger repulsion between a fluorine and a chlorine atoms (not between the same atoms) in the carbynes with mixed haloen atoms leads to a C_1 structure. Considerable distortions by the extra electron(s) on the

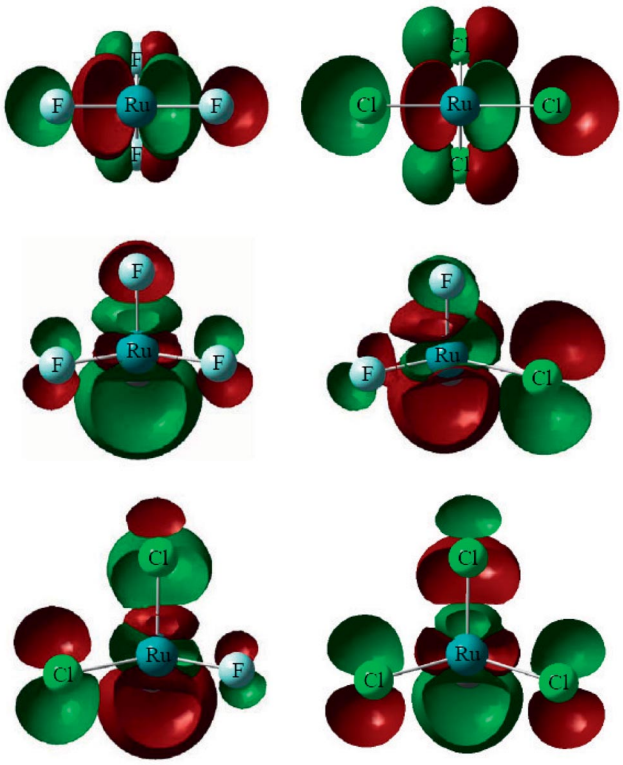

Figure 7. The HOMOs of CF_2=RuF_2, CCl_2=$RuCl_2$, FC≡RuF_3, ClC≡RuF_2Cl, ClC≡$RuFCl_2$, and ClC≡$RuCl_3$ in their triplet ground states looking from the Ru side. Notice the nodal planes between the halogen atoms. The extra electrons on the Ru atom contribute bonding and *anti*-bonding characters between halogen atoms, and thereby the extra electrons greatly affect the structure of the complex. Notice the allene-type carbene structure and the two carbyne halogen atoms bonded to Ru push apart, lowering the molecular symmetry.

metal atom are also observed from small Re and Os carbyne complexes, such as methylidyne trihydrides, HC≡MH_3.[11] The metal–hydrogen bonds are not the same: one is much longer and more inclined, resulting in observation of a strong Os–H stretching absorption with unusually low frequency.

Ru + $CHCl_3$

Infrared spectra of the products from Ru and $CHCl_3$ isotopomer reactions in the C–H stretching, C–D stretching, and HCRu bending regions are illustrated in Figure S1 (Supporting Information). The **m** absorptions increase about 20% on visible photolysis but are almost depleted on UV photolysis. They recover to about 40% of the original intensity on a second visible photolysis, but decrease again on the following UV irradiation. On the other hand, **y** absorptions are relatively much weaker. They decrease 10% on visible photolysis but increase about 30% on UV irradiation. As a result, the **m** and **y** absorptions show a photoreversible pattern on alternating visible and UV UV photolysis, suggesting that the **m** and **y** absorptions arise from two products which are photochemically inter-convertible analogous to several other methane and halomethane systems.[15]

Parallel to the tetrahalomethane cases described above, the insertion product is much less stable than the carbene and carbyne products; $CHCl_2$–RuCl(Q), CHCl=$RuCl_2$(T), and HC≡$RuCl_3$(T) are 62, 98, and 90 kcal/mol lower in energy than the reactants, respectively. The observed frequencies of the **m** and **y** absorptions are summarized in Table 2. Strong **m** absorptions are split by the matrix as are their ^{13}C counterparts ($^{12}C/^{13}C$ ratios of 1.006, 1.006, and 1.007). They are designated to A′ HCRu bending mode of CHCl=$RuCl_2$ on the basis of the frequencies and good agreement with the predicted value (Table S3). The insertion and carbyne complexes do not have strong bands in this region.

Strong **m** absorptions are also observed at 870.6 and 862.9 cm^{-1}, the D counterpart at 761.5 cm^{-1} (not shown, H/D ratio of 1.133), and the ^{13}C counterparts at 846.0 and 837.3 cm^{-1} ($^{12}C/^{13}C$ ratios of 1.029 and 1.031). They are assigned to the C–Cl stretching mode on the basis of the frequencies and a relatively small D and a substantial ^{13}C shifts. Another **m** absorption at 701.8 cm^{-1} (not shown) has its D counterpart at 580.6 cm^{-1} (H/D ratio of 1.209), but the ^{13}C counterpart is believed covered by a precursor absorption. It is assigned to the A" HCRu bending mode of CHCl=$RuCl_2$. The observed frequencies correlate with the predicted frequencies (Table S3) and substantiate formation of the methylidene product, CHCl=$RuCl_2$.

A weak **y** absorption is observed at 3065.3 cm^{-1} in the C–H stretching region and the D counterpart at 2312.4 cm^{-1} (H/D ratio of 1.326), but the ^{13}C counterpart is unfortunately covered by a precursor band. The high C–H stretching frequency suggests a multiple carbon–ruthenium bond providing higher s character to the C–H bond.[6,29] We assign the **y** absorption at 3065.3 cm^{-1} to the C–H stretching band of HC≡$RuCl_3$. Another **y** absorptions is observed at 586.1 cm^{-1}, and its D and ^{13}C counterparts at 470.7 and 571.7 cm^{-1} (H/D and $^{12}C/^{13}C$ ratios of 1.245 and 1.025). On the basis of the frequency and large D shift,

Table 2. Frequencies of product absorptions observed from reactions of Ru and $CHCl_3$ isotopomers in excess argon.[a]

	$CHCl_3$	$CDCl_3$	$^{13}CHCl_3$	Description
m	1158.6, 1153.3, 1143.5	covered[b]	1151.8,1146.1, 1135.8	A′ HCRu bend
	870.6, 862.9	761.5	846.0, 837.3	A′ C–Cl str.
	701.8	580.6	covered[b]	A′′ HCRu bend
y	3077.7	2294.7	covered	A_1 C–H str.
	586.1	470.4	571.7	E HCRu bend

[a] All frequencies are in cm^{-1}. Description gives major coordinate. [b] Covered by precursor absorption.

it is assigned to the degenerate HCRu bending mode of $HC{\equiv}RuCl_3$. Table S4 shows that the C–H stretching and HCRu bending bands are in fact the strongest ones predicted in our observation range. This agreement between the observed and predicted vibrational characteristics supports formation of the Ru carbyne complex.

Ru + CH_2F_2

Figure 8 shows the CH_2F_2 and CD_2F_2 spectra, and the **m** product absorptions are much stronger relative to the **y** absorptions. The **m** absorptions increase slightly (less than 5%) and about 20% on visible and UV photolysis, respectively. They increase further 5% on full arc photolysis. The **y** absorptions decrease slightly (≈ 10%) on visible irradiation but increase about 20% on UV photolysis and further increase 10% on subsequent full arc photolysis.

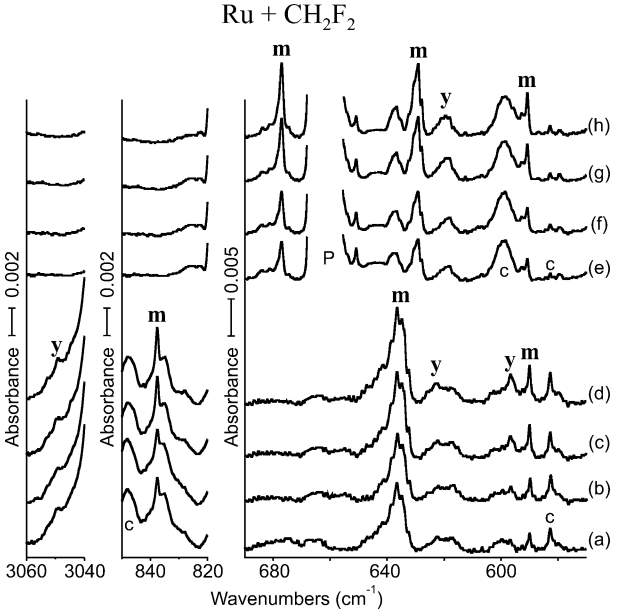

Figure 8. IR spectra in the regions of 3060–3040, 850–820, and 690–570 cm^{-1} for laser-ablated Ru atoms co-deposited with CH_2F_2 and CD_2F_2 in excess argon at 8 K and their variation. (a) Ru + 0.5% CH_2F_2 in Ar co-deposited for 1 h. (b) As (a) after photolysis ($\lambda > 420$ nm). (c) As (b) after photolysis ($240 < \lambda < 380$ nm). (d) As (c) after photolysis ($\lambda > 220$ nm). (e) Ru + 0.5% CD_2F_2 in Ar co-deposited for 1 h. (f) As (e) after photolysis ($\lambda > 420$ nm). (g) As (f) after photolysis ($240 < \lambda < 380$ nm). (h) As (g) after photolysis ($\lambda > 220$ nm); **m** and **y** denote the product absorption groups; P and c show the precursor band and common absorption in the CH_2F_2 spectra.

Similar to the tetra- and trihalomethane cases, the insertion product is less stable than the carbene and carbyne complexes. CH_2F–RuF(Q), $CH_2{=}RuF_2$(T), and $HC{\equiv}RuHF_2$(S) are 36, 60, and 51 kcal/mol lower than the reactants, respectively. A strong **m** absorption is observed at 837.5 cm^{-1} and its D counterpart at 677.0 cm^{-1} (H/D ratio of 1.237). The frequency and large D shift lead to an assignment to the CH_2 wagging mode of $CH_2{=}RuF_2$. Calculation results also show that the insertion and carbyne (Table S6, Supporting Information) products would not have observably strong bands in this frequency region. Another strong **m** absorption at 636.6 cm^{-1} has its D counterpart at 629.1 cm^{-1} (H/D ratio of 1.022) is assigned to the *anti*-symmetric RuF_2 stretching mode on the basis of the frequency and the relatively small D shift. The **m** absorption at 590.0 cm^{-1} has its D counterpart at 590.7 cm^{-1} and is assigned to the symmetric RuF_2 stretching mode. The observed frequencies are consistent with the predicted frequencies of the strongest (Table S5) substantiates formation of $CH_2{=}RuF_2$.

The **y** absorption at 3049.4 cm^{-1} on the blue side of the precursor C–H stretching band is most probably the C–H stretching band of $HC{\equiv}RuHF_2$, but unfortunately the D counterpart is covered by a precursor band. Another **y** absorption observed at 622.6 cm^{-1} has its D counterpart at 619.6 cm^{-1} (H/D ratio of 1.005), and due to its small D shift, it is assigned to the RuF_2 *anti*-symmetric stretching mode. The **y** absorption observed at 596.6 cm^{-1} is assigned to the RuF_2 symmetric stretching mode while its D counterpart is believed covered by other spectra features. The observed **y** absorptions, consistent with the computed vibrational characteristics, support the formation of $HC{\equiv}RuHF_2$.

Ru + CH_2FCl

Shown in Figure S2 are the CH_2FCl and CD_2FCl spectra in the C–H stretching, CH_2 wagging, and the low frequency regions. Here, the **m** absorptions are relatively stronger. They increase about 10% on the first visible irradiation, but decrease 40% on subsequent UV photolysis, and increase about 25% on the following visible photolysis, but decrease on the next UV photolysis. In contrast the **y** absorptions decrease to a half in intensity on visible irradiation, but increase 70% on subsequent UV photolysis (20% increase from the original intensity). They again decrease to a half on the following visible photolysis and recover in the next UV irradiation. These alternating changes in intensity on visible and UV photolysis again revealed a photo-reversible system, suggesting that the **m** and **y** absorptions originate from products inter-convertible by α-H transfer.[15]

$$Ru + CH_2FCl \rightarrow CH_2Cl{-}RuF^* \text{ or } CH_2F{-}RuCl^* \rightarrow CH_2{=}RuFCl \leftrightarrow HC{\equiv}RuHFCl$$

The plausible insertion complexes are again less stable than the carbene and carbyne complexes; CH_2Cl–RuF(T), CH_2F–RuCl(T), $CH_2{=}RuFCl$(T), and $HC{\equiv}RuHFCl$(S) are 54, 54, 73, and 64 kcal/mol lower in energy than the reactants. The **m** absorption at 884.3 cm^{-1} has its D counterpart at 678.4 cm^{-1} (H/D ratios of 1.304) and is assigned to the CH_2 wagging mode of $CH_2{=}RuFCl$ on the basis of the frequency and large D shift. The strong **m** absorption at 609.2 cm^{-1} shows a D shift of only –0.8 cm^{-1} (H/D ratio of 1.001) and is assigned to the Ru–F stretching mode due to the small D shift. A weak **m** absorption is also observed at 1341.2 cm^{-1} and assigned to the CH_2 scissoring mode. The

observed absorptions are in fact the bands predicted strongest (Table S6), and the good agreement between the observed and predicted frequencies substantiates formation of CH_2=RuFCl.

The **y** absorption at 3064.0 cm^{-1} is assigned to the C–H stretching mode of HC≡RuHFCl while the D counterpart is believed covered by a precursor band. The **y** absorption at 637.1 cm^{-1} is assigned to the HRuC bending mode on the basis of its frequency while the D counterpart located too low in frequency is not observed. Another **y** absorption at 589.1 cm^{-1} shows a D shift of –6.3 cm^{-1} (H/D ratio of 1.011) and is assigned to the Ru–F stretching mode. The observed frequencies show a good agreement with the calculated values and support the formation of the carbyne complex, HC≡RuHFCl.

Ru + CH_2Cl_2

The spectra of CH_2Cl_2 isotopomer reaction products are given in Figure S3. The relatively stronger **m** absorptions increase almost 30% on visible photolysis, but decrease about 70% on UV irradiation, and recover to the original intensity on the following visible photolysis. Again the **y** absorptions show opposite change in intensity on photolysis; and these two products are photo-reversible through α-H transfer.

$$Ru + CH_2Cl_2 \rightarrow CH_2Cl–RuCl^* \rightarrow CH_2{=}RuCl_2 \leftrightarrow HC{\equiv}RuHCl_2$$

The insertion complex is again less stable than the carbene and carbyne complexes; CH_2Cl–RuCl(T), CH_2=$RuCl_2$(T), and HC≡$RuHCl_2$(S) are 67, 84, and 78 kcal/mol lower in energy than the reactants. The **m** absorption at 1333.9 cm^{-1} (Table 3) has its ^{13}C counterpart at 1325.6 cm^{-1}, but the D counterpart is covered by a precursor absorption. It is assigned to the CH_2 scissoring mode of CH_2=$RuCl_2$ on the basis of the frequency and isotopic shifts. The strong **m** absorption at 848.3 cm^{-1} shows D and ^{13}C isotopic shifts of –172.2 and –7.9 cm^{-1} (H/D and $^{12}C/^{13}C$ ratios of 1.255 and 1.009), respectively, and is assigned to the CH_2 wagging mode on the basis of the frequency and isotopic shifts. The **m** absorption at 411 cm^{-1}, close to our observation limit, has its D and ^{13}C counterparts at 406 and 411 cm^{-1} (all not shown) and it is assigned to the Ru–Cl *anti*-symmetric stretching mode. The observed frequencies correlate with the computed values and support the formation of CH_2=$RuCl_2$.

A broad **y** absorption at 3056.7 cm^{-1} has its D and ^{13}C counterparts at 2299.6 and 3043.3 cm^{-1} (H/D and $^{12}C/^{13}C$ ratios of 1.329 and 1.004), respectively, and it is assigned to the C–H stretching mode of HC≡$RuHCl_2$. A weak **y** absorption is observed at 618.5 cm^{-1} and the ^{13}C counterpart at 617.1 cm^{-1}. It is assigned to the A′ HCRu bending mode while the D counterpart located too low in frequency to observe. Another weak **y** absorption at 592.6 cm^{-1} with its D counterpart at 464.5 cm^{-1} is assigned to the A" HCRu bending mode.

Carbyne C–H Stretching Band

The diagnostic carbyne C–H stretching absorptions of the Ru complexes are observed in the $CHCl_3$, CH_2F_2, CH_2FCl, and CH_2Cl_2 spectra. The small methylidyne complexes with no interfering ligand chromophores and the simple precursor absorptions in this region allow observation of the weak but important C–H stretching band of the H–C≡M moiety.[9,11] The frequencies about 200 cm^{-1} higher than those of saturated hydrocarbons signify the adjacent carbon–rutheium triple bond, which increases the s character of the C–H bond.[29] The close relation between the methylidyne C–H stretching frequency and the amount of s character was examined in the previous Re and Os studies.[11]

The NBO[30] s characters of the Ru carbyne C–H bonds of HC≡$RuCl_3$, HC≡$RuHF_2$, HC≡RuHFCl, and HC≡$RuHCl_2$ (50.92, 49.95, 48.30, and 47.89%) are considerably higher than that of ethane (23.46%) and consistent with the observed high frequencies of 3065–3049 cm^{-1}. The s characters of the small Ru carbyne complexes, however, are in fact even higher than that of acetylene (47.82%), whose antisymmetric C–H stretching frequency is 3284 cm^{-1} and the IR-inactive symmetric stretching mode is even 90 cm^{-1} higher.[31] The trends between the carbyne C–H stretching frequency and the s character observed in the studies of reactions of Re and Os with methane and methyl halides[11] do not appear to hold for these Ru multihalocarbynes.

Table 3. Frequencies of product absorptions observed from reactions of Ru and CH_2X_2 isotopomers in excess argon.[a]

	CH_2F_2	CD_2F_2	CH_2FCl	CD_2FCl	CH_2Cl_2	CD_2Cl_2	$^{13}CH_2Cl_2$	Description
m					1333.9	covered[b]	1325.6	CH_2 scis.
	837.5	677.0	844.3	678.4	848.3	676.1	840.4	CH_2 wag
	636.6	629.1	609.2	608.4	410.8	405.9	412.9	RuX_2 asym. str.
	590.0	590.7						RuX_2 sym. str.
y	3049.4	covered[b]	3064.0	covered[b]	3056.7	2299.6	3043.3	C–H str.
			637.1		618.5		617.1	HRuC bend
					592.6	464.5		HCRu bend
	622.6	619.6	589.1	582.8				RuF_2 asym. str.
	596.7	covered[b]						RuF_2 sym. str.

[a] All frequencies are in cm^{-1}. Description gives major coordinate. **m** and **y** stand for methylidene and methylidyne products, respectively. [b] Covered by precursor absorption.

Structures of Tri- and Dihalomethane Products

Figure S4 (Supporting Information) illustrates the optimized structures of carbenes and carbynes prepared in reactions of Ru with tri- and dihalomethanes. The structures of the carbenes are similar to those of carbene tetrahalides shown in Figure 6. The carbyne HC≡$RuCl_3$(T) reveals the only C_{3v} structure. The other carbynes all have substantially distorted structures, and the most distorted is the difluoro carbyne (HC≡$RuHF_2$). In the dihalocarbyne structures, the H–Ru bond is inclined to the carbon atom, and the H, C, Ru, and two halogen atoms form a nearly planar structure [ϕ(FRuCF), ϕ(ClRuCF), and ϕ(ClRuCCl) are 170.9, 171.2, and 172.3°, respectively]. Substitution of the chlorine atom bonded to the carbon atom with hydrogen greatly reduces the carbon–ruthenium bond length; the C≡Ru bonds of the di- and trihalocarbynes are considerabley shorter (≈ 0.05 Å) than those of tetrahalocarbynes shown in Figure 6.

The HOMOs of HC≡$RuCl_3$(T), HC≡$HRuF_2$(S), HC≡RuHFCl(S), and HC≡$RuHCl_2$(S) illustrated in Figure S5 show that the extra electron pair greatly affects the structures of the carbyne complexes. The nodal planes intersect the X–Ru–X bonds, providing *anti*-bonding character and pushing the two halogen atoms apart, explaining the near planar structure formed by H, C, Ru, and two halogen atoms. This shows again how important the extra electrons on the metal atom are in determining the structure of the complex.

Ru + CH_3F

Figure 9 depicts the CH_3F spectra for product absorptions including the Ru–F stretching region. The **i** absorptions decrease to one third of original intensity on visible irradiation and recover on UV photolysis. The **y** absorptions increase 60% on the first visible irradiation and another 60% on the following UV irradiation. They increase 50% more in the subsequent visible photolysis and remain unchanged in the next UV irradiation.

Unlike the di-, tri-, and tetrahalomethane cases described above, the insertion and carbyne complexes are more stable than the carbene complex in the Ru + CH_3F system; CH_3–RuF(Q), CH_2=RuHF(T), and HC≡RuH_2F(S) are 49, 39, and 45 kcal/mol lower in energy than the reactants. The **i** absorption at 574.2 cm^{-1} (Table 4) shows very small D and ^{13}C isotopic shifts of –2.1 and –0.6 cm^{-1} and is assigned to the Ru–F stretching mode of the insertion product, CH_3–RuF. The carbene and carbyne complexes would give much larger isotopic shifts for the Ru–F stretching mode and the predicted frequencies also do not match (Tables S7–S9). The weak absorption at 547.5 cm^{-1} observed between the stronger **y** absorptions has a D counterpart at 468.8 cm^{-1} (H/D ratio of 1.168) and is designated to the C–Ru stretching mode of CH_3–RuF. Another **i** absorption at 519.4 cm^{-1} shows a ^{13}C shift of –13.6 cm^{-1} and is assigned to the A′ CH_3 rocking mode. The observed vibrational characteristics consistent with the calculated values for CH_3–RuF (Table S7) support the formation of the insertion product.

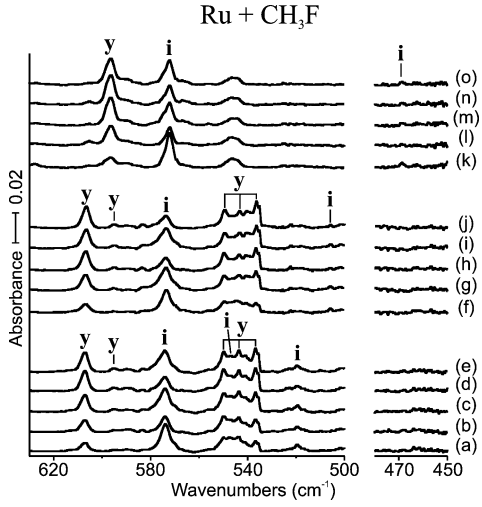

Figure 9. IR spectrum in the region of 630–500 and 480–450 cm^{-1} for laser-ablated Ru atoms co-deposited with CH_3F isotopomers in excess argon at 8 K and their variation. (a) Ru + 0.5% CH_3F in Ar co-deposited for 1 h. (b) As (a) after photolysis ($\lambda > 420$ nm). (c) As (b) after photolysis ($240 < \lambda < 380$ nm). (d) As (c) after photolysis ($\lambda > 420$ nm). (e) As (d) after photolysis ($240 < \lambda < 380$ nm). (f) Ru + 0.5% $^{13}CH_3F$ in Ar co-deposited for 1 h. (g) As (f) after photolysis ($240 < \lambda < 380$ nm). (h) As (g) after photolysis ($\lambda > 420$ nm). (i) As (h) after photolysis ($240 < \lambda < 380$ nm). (j) As (i) after photolysis ($\lambda > 420$ nm). (k) Ru + 0.5% CD_3F in Ar co-deposited for 1 h. (l) As (k) after photolysis ($\lambda > 420$ nm). (m) As (l) after photolysis ($240 < \lambda < 380$ nm). (n) As (m) after photolysis ($\lambda > 420$ nm). (o) As (n) after photolysis ($240 < \lambda < 380$ nm); **i** and **y** denote the product absorption groups.

Table 4. Frequencies of product absorptions observed from reactions of Ru and methyl fluoride in excess argon.[a]

	CH_3F	CD_3F	$^{13}CH_3F$	Description
i	574.2	572.1	573.6	A′ Ru–F str.
	547.5	468.8		A′ C–Ru str.
	519.4		505.8	A′ CH_3 rock
y	607.1	596.5	606.8	A′ Ru–F str.
	595.4		595.0	A′′ RuH_2 twist
	549.8, 543.6, 536.8		549.6, 543.4, 536.5	A′ RuH_2 wag

[a] All frequencies are in cm^{-1}. Description gives major coordinate. **i** and **y** stand for insertion and methylidyne products, respectively.

The strong **y** absorption at 607.1 cm^{-1} shows D and ^{13}C shifts of –10.6 and –0.3 cm^{-1} and is assigned to the Ru–F stretching mode of the carbyne complex (HC≡RuH_2F) on the basis of the small isotopic shifts and a good agreement with the calculated values (Table S9). The observed **y** absorptions do not fit with the predicted vibrational characteristics for the insertion and carbene products (Tables S7 and S8). The relatively weak **y** absorption at 595.4 cm^{-1} has its ^{13}C counterpart at 595.0 cm^{-1}, but the D counterpart is too low in frequency to observe. We assign it to the A′′ RuH_2 twisting mode of HC≡RuH_2F. A group of **y** absorptions split by the matrix are observed at 549.8, 543.6, 536.8 cm^{-1} with the ^{13}C counterparts at 549.6, 543.4,

536.5 cm^{-1}, and the D counterparts are again too low in frequency to observe. The frequencies and the small ^{13}C and large D shifts lead to an assignment to the ReH_2 wagging mode. While the C–H stretching absorption of the carbyne product is not observed, most probably due to masking by the precursor C–H band. The observed vibrational characteristics in the low frequency region match very well with the computed values for $HC{\equiv}RuH_2F(S)$, supporting formation of the carbyne complex.

Ru + CH_4

Figure 10 illustrates the CH_4 reaction product spectra in the Ru–H and Ru–D stretching regions. Unlike the halomethane systems, only one type of absorptions marked "**i**" are observed. The broad, relatively strong absorption at 1918.1 cm^{-1} (Table 5), overlapped with the weak Ru(CO) absorption,[32] shows essentially no ^{13}C shift, and the D counterpart is observed at 1387.3 cm^{-1} (H/D ratio of 1.383). The observed frequencies are close to the RuH_2 and RuD_2 molecule stretching frequencies (1821.0 1312.2 cm^{-1}),[33] and the single intensive absorption strongly suggests the formation of a product with a single Ru–H bond, namely CH_3–RuH.

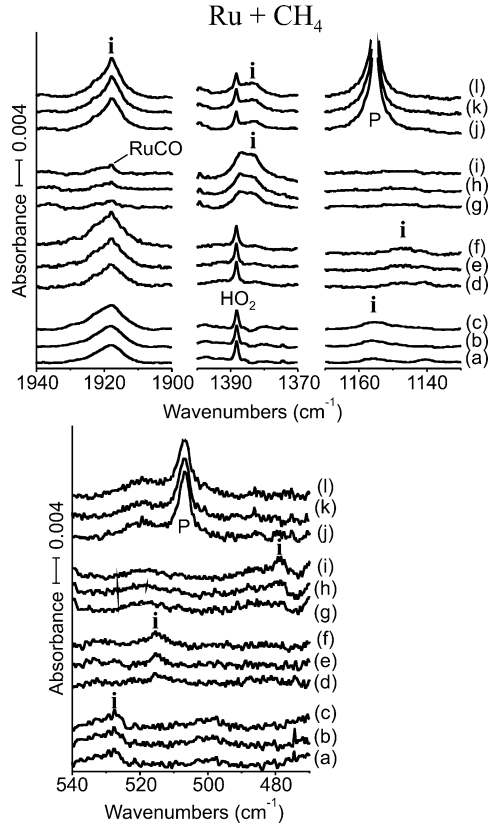

Figure 10. IR spectra in the regions of 1940–1900, 1400–1370, 1170–1130, and 540–470 cm^{-1} for laser-ablated Ru atoms co-deposited with CH_4 isotopomers in excess argon at 8 K and their variation. (a) Ru + 0.5% CH_4 in Ar co-deposited for 1 h. (b) As (a) after photolysis ($\lambda > 420$ nm). (c) As (b) after photolysis ($240 < \lambda < 380$ nm). (d) Ru + 0.5% CD_4 in Ar co-deposited for 1 h. (e) As (d) after photolysis ($\lambda > 420$ nm). (f) As (e) after photolysis ($240 < \lambda < 380$ nm). (g) Ru + 0.5% $^{13}CH_4$ in Ar co-deposited for 1 h. (h) As (g) after photolysis ($\lambda > 420$ nm). (i) As (h) after photolysis ($240 < \lambda < 380$ nm). (j) Ru + 0.5% CH_2D_2 in Ar co-deposited for 1 h. (k) As (j) after photolysis ($\lambda > 420$ nm). (l) As (k) after photolysis ($240 < \lambda < 380$ nm); **i** and P denote the product and precursor absorptions, respectively.

Table 5. Frequencies of product absorptions observed from reactions of Ru and methane in excess argon.[a]

	CH_4	CD_4	$^{13}CH_4$	CH_2D_2	Description
i	1918.1	1383.0	1918.1	1923.2, 1383.0	Ru–H str.
	1156.5	covered[b]	1147.6		CH_3 def.
	528.0	478.5	515.1	486.2	C–Ru str.

[a] All frequencies are in cm^{-1}. Description gives major coordinate. **i** stands for insertion product. Frequencies and intensities are computed with 6-311++G(3df, 3pd) for harmonic calculations except where otherwise noted, and the SDD core potential and basis set are used for Ru. Intensities are calculated with B3LYP, and frequencies and intensities are in cm^{-1} and km/mol. CH3–RuH has a Cs structure at all levels of calculation performed in this study. The symmetry notations are based on the Cs structure. [b] Calculated anharmonic frequencies.

A weak **i** absorption is also observed at 1156.5 cm^{-1} and its ^{13}C counterpart at 1147.6 cm^{-1}. It is assigned to the CH_3 deformation mode, and the D counterpart is unfortunately covered by a precursor absorption. Another weak **i** absorption at 528 cm^{-1} shows D and ^{13}C shifts of –49.5 and –12.9 cm^{-1} (H/D and $^{12}C/^{13}C$ ratios of 1.103 and 1.025). It is assigned to the C–Ru stretching mode on the basis of the sizeable ^{13}C shift. The observed vibrational characteristics correlate well with the predicted values and support the formation of the insertion complex in the reaction of Ru with CH_4. This result is also consistent with the relative energies of the plausible products. The insertion product is more stable than the carbene and carbyne complexes: CH_3–RuH(T) and $CH_2{=}RuH_2(S)$ are 14, and 8 kcal/mol lower than the reactants, but $HC{\equiv}RuH_3(S)$ is 8 kcal/mol higher.

Structrures of Methyl Fluoride and Methane Products

Figure 11 gives optimized structures of CH_3–RuF, $HC{\equiv}RuH_2F$, and CH_3–RuH. Notice that the C–Ru bond of $HC{\equiv}RuH_2F$ is much shorter than those of CH_3–RuF and CH_3–RuH due to the carbon–Ru multiple bond, but comparable to those of dihalocarbynes shown in Figure S4. The distorted structure of the monofluorocarbyne (the angles C–Ru–F and H–Ru–H are 86.4 and 81.1°), $HC{\equiv}RuH_2F$, is compared with the structures of other carbynes identified in this study. Our TOC graphic shows the HOMO of $HC{\equiv}RuH_2F$. There is a nodal plane between the F and H atoms bonded to the Ru atom. The extra electron pair pushes the F and H atoms apart and draws the two H atoms closer to each other, leading to the unique structure.

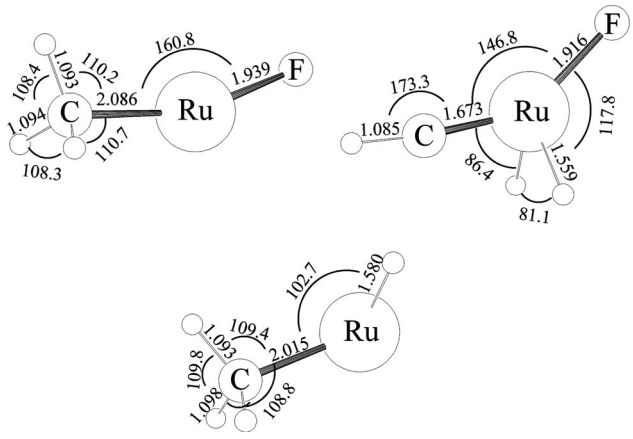

Figure 11. Optimized molecular structures of the identified Ru insertion and methylidyne complexes in the CH_3F and CH_4 spectra. The structures are calculated with B3LYP/6-311++G(3df,3pd), and the SDD core potential and basis set are used for Ru. They all have a C_s structure. The bond lengths and angles are in Å and degrees.

Conclusions

Reactions of laser-ablated Ru atoms with halomethanes and methane have been carried out. Carbene and carbyne products (CX_2=RuX_2 and XC≡RuX_3, X = F, Cl or H) are formed in reactions of tetra- and trihalomethanes, whereas the insertion and carbyne products are identified from reaction of methyl fluoride, and only the insertion complex (CH_3–RuH) is produced in the reaction with methane. Calculations also show that the insertion product (CX_3–RuX) from the reaction of a halomethane is less stable than the carbene and carbyne complexes, but the insertion complex becomes the most stable product in the reactions of methyl fluoride and methane. The driving force here is for the initial energized inserted species to rearrange into the most stable product, and when multiple halogen atoms are present, these transfer to the metal center thus forming stronger bonds.

The diagnostic carbyne C–H and C–X absorptions are observed on the blue side of the precursor C–H and C–X bands. The exceptionally high C–X stretching frequencies are due to the fact that the carbyne C–X stretching mode is essentially a X–C–Ru anti-symmetric stretching mode, and as a result, interaction between the C–X and C≡Ru stretching motions leads to an increase in the frequency.

The structures of the identified Ru carbynes are highly distorted and show a large variation with the ligands while the carbenes all have an allene-type structure. The distorted Ru carbyne structures follow the small Re and Os carbynes.[11] Evidently the extra electron pair on the Ru atom plays an important role in the distinct molecular structures. The present study reveals that the HOMOs of the carbyne complexes provide important clues for the distorted structures.

Experimental Section

Methods: Laser-ablated Ru atoms (Metallium, Inc.) were treated with CF_4 (Dupont), CF_3Cl,[34] CF_2Cl_2, $CFCl_3$, CCl_4, $^{13}CCl_4$, $CHCl_3$, $CDCl_3$, $^{13}CHCl_3$, CH_2F_2,[34] CH_2FCl,[34] CH_2Cl_2, CD_2Cl_2, $^{13}CH_2Cl_2$, CH_3F (Matheson), CD_3F (synthesized from CD_3Br and HgF_2), $^{13}CH_3F$ (Cambridge Isotopic Laboratories, 99%), CH_4 (Matheson, UHP), $^{13}CH_4$, CD_4, CH_2D_2 (Cambridge Isotopic Laboratories) in excess argon during condensation at 8 K using a closed-cycle refrigerator (Air Products HC-2).[35] Reagent gas mixtures ranged 0.5–2.0% in argon. After reaction, infrared spectra were recorded at a resolution of 0.5 cm^{-1} using a Nicolet 550 spectrometer with an MCT-B detector. Samples were later irradiated for 20-min periods by a mercury arc street lamp (175 W) with the globe removed and a combination of optical filters, and subsequently annealed to allow further reagent diffusion.[35]

Supporting Information (see footnote on the first page of this article): contains tables of calculated product frequencies, infrared spectra, and product structures and molecular orbitals.

Acknowledgments

We gratefully acknowledge financial support from the National Science Foundation (US), Grant CHE 03-52487 to L. A., and support from the Korea Institute of Science and Technology Information (KISTI), Grant KSC-2006-S00-2014.

[1] a) R. R. Schrock, *Chem. Rev.* **2002**, *102*, 145; b) J. W. Herndon, *Coord. Chem. Rev.* **2007**, *251*, 1158; c) J. W. Herndon, *Coord. Chem. Rev.* **2006**, *250*, 1889; d) J. W. Herndon, *Coord. Chem. Rev.* **2005**, *249*, 999; e) J. W. Herndon, *Coord. Chem. Rev.* **2004**, *248*, 3.

[2] a) E. O. Fischer, G. Kreis, C. G. Kreiter, J. Müller, G. Huttner, H. Lorenz, *Angew. Chem. Int. Ed. Engl.* **1973**, *12*, 564; b) S. J. McLain, C. D. Wood, L. W. Messerle, R. R. Schrock, F. J. Hollander, W. J. Youngs, M. R. Churchill, *J. Am. Chem. Soc.* **1978**, *100*, 5962.

[3] a) R. H. Grubbs (Ed.), *Handbook of Metathesis*, Wiley-VCH, Weinheim, Germany, **2003**; vol. 1–3; b) U. H. F. Bunz, *Chem. Rev.* **2000**, *100*, 1605.

[4] a) M. A. Gallop, W. R. Roper, *Adv. Organomet. Chem.* **1986**, *25*, 121; b) J. N. Coalter, J. C. Bollinger, O. Eisenstein, K. G. Caulton, *New J. Chem.* **2000**, *24*, 925; c) M. S. Sanford, L. M. Henling, M. W. Day, R. H. Grubbs, *Angew. Chem. Int. Ed.* **2000**, *39*, 3451; d) P. Gonzales-Herrero, B. Weberndorfer, K. Ilg, J. Wolf, H. Werner, *Angew. Chem. Int. Ed.* **2000**, *39*, 3266; e) P. Gonzales-Herrero, B. Weberndorfer, K. Ilg, J. Wolf, H. Werner, *Organometallics* **2001**, *20*, 3672; f) D. Amoroso, J. L. Snelgrove, J. C. Conrad, S. D. Droulin, G. P. A. Yap, D. E. Fogg, *Adv. Synth. Catal.* **2002**, *344*, 757 (Ru carbyne synthesis).

[5] a) H. Fischer, P. Hofmann, F. R. Kreissl, R. R. Schrock, U. Schubert, K. Weiss, *Carbyne Complexes*, VCH Publishers, New York, **1988**; b) M. A. Gallop, W. R. Roper, *Adv. Oranomet. Chem.* **1986**, *25*, 121; c) P. F. Engel, M. Pfeffer, *Chem. Rev.* **1995**, *95*, 2281.

[6] W. A. Nugent, J. M. Mayer, *Metal-Ligand Multiple Bonds*, John Wiley & Sons, New York, **1988**.

[7] D. Barnes, D. A. Gillett, A. J. Merer, G. F. Metha, *J. Chem. Phys.* **1996**, *105*, 6168 (W≡CH near-IR spectrum).

[8] a) M. Barnes, A. J. Merer, G. F. Metha, *J. Mol. Spectrosc.* **1997**, *181*, 168 (Ti≡CH); b) L. Sari, Y. Yamaguchi, H. F. Schaefer III, *J. Chem. Phys.* **2001**, *115*, 5932 (Ge≡CH); c) A. Kalemos, T. H. Dunning Jr, J. F. Harrison, A. Mavridis, *J. Chem. Phys.* **2003**, *119*, 3745 (Ti≡CH).

[9] J. Manna, R. F. Dallinger, V. M. Miskowski, M. D. Hopkins, *J. Phys. Chem. B* **2000**, *104*, 10928 (H–C≡W group frequency).

[10] J. T. Lyon, H.-G. Cho, L. Andrews, *Organometallics* **2007**, *26*, 6373(Cr, Mo, W + CHX_3, CX_4).

[11] a) H.-G. Cho, L. Andrews, *Organometallics* **2007**, *26*, 4098; b) H.-G. Cho, L. Andrews, *Inorg. Chem.* **2008**, ASAP (R + al-

kanes); c) H.-G. Cho, L. Andrews, *Organometallics* **2008**, in press (Os + alkanes).
[12] J. T. Lyon, H.-G. Cho, L. Andrews, H.-S. Hu, J. Li, *Inorg. Chem.* **2007**, *46*, 8728 (Re + CHX_3, CX_4).
[13] a) H. A. Jahn, E. Teller, *Proc. R. Soc. London, Ser. A* **1937**, *161*, 220; b) E. Teller, *A historical note*, in *The Jahn–Teller Effect in Molecules and Crystals* (Ed.: R. Engelman), Wiley-Interscience, London, **1972**.
[14] a) K. R. Campos, *Chem. Soc. Rev.* **2007**, *36*, 1069; b) M. M. Díaz-Requejo, T. R. Belderrain, M. C. Nicasio, P. Pérez, *Dalton Trans.* **2006**, 5559.
[15] L. Andrews, H.-G. Cho, *Organometallics* **2006**, *25*, 4040, and references cited therein (review article).
[16] K. N. Kudin, J. C. Burant, J. M. Millam, S. S. Iyengar, J. Tomasi, V. Barone, B. Mennucci, M. Cossi, G. Scalmani, N. Rega, G. A. Petersson, H. Nakatsuji, M. Hada, M. Ehara, K. Toyota, R. Fukuda, J. Hasegawa, M. Ishida, T. Nakajima, Y. Honda, O. Kitao, H. Nakai, M. Klene, X. Li, J. E. Knox, H. P. Hratchian, J. B. Cross, C. Adamo, J. Jaramillo, R. Gomperts, R. E. Stratmann, O. Yazyev, A. J. Austin, R. Cammi, C. Pomelli, J. W. Ochterski, P. Y. Ayala, K. Morokuma, G. A. Voth, P. Salvador, J. J. Dannenberg, V. G. Zakrzewski, S. Dapprich, A. D. Daniels, M. C. Strain, O. Farkas, D. K. Malick, A. D. Rabuck, K. Raghavachari, J. B. Foresman, J. V. Ortiz, Q. Cui, A. G. Baboul, S. Clifford, J. Cioslowski, B. B. Stefanov, G. Liu, A. Liashenko, P. Piskorz, I. Komaromi, R. L. Martin, D. J. Fox, T. Keith, M. A. Al-Laham, C. Y. Peng, A. Nanayakkara, M. Challacombe, P. M. W. Gill, B. Johnson, W. Chen, M. W. Wong, C. Gonzalez, J. A. Pople, *Gaussian 03*, Revision B.04, Gaussian Inc., Pittsburgh, PA, **2003**.
[17] a) A. D. Becke, *J. Chem. Phys.* **1993**, *98*, 5648; b) C. Lee, Y. Yang, R. G. Parr, *Phys. Rev. B* **1988**, *37*, 785.
[18] K. Raghavachari, G. W. Trucks, *J. Chem. Phys.* **1989**, *91*, 1062.
[19] D. Andrae, U. Haeussermann, M. Dolg, H. Stoll, H. Preuss, *Theor. Chim. Acta* **1990**, *77*, 123.
[20] K. Burke, J. P. Perdew, Y. Wang, in *Electronic Density Functional Theory: Recent Progress and New Directions* (Eds.: J. F. Dobson, G. Vignale, M. P. Das), Plenum, **1998**.
[21] A. P. Scott, L. Radom, *J. Phys. Chem.* **1996**, *100*, 16502.
[22] M. P. Andersson, P. L. Uvdal, *J. Phys. Chem. A* **2005**, *109*, 3937.
[23] a) D. E. Milligan, M. E. Jacox, *J. Chem. Phys.* **1968**, *48*, 2265; b) M. E. Jacox, D. E. Milligan, *J. Chem. Phys.* **1970**, *53*, 2688.
[24] a) C. E. Smith, D. E. Milligan, M. E. Jacox, *J. Chem. Phys.* **1971**, *54*, 2780; b) F. T. Prochaska, L. Andrews, *J. Chem. Phys.* **1978**, *68*, 5577.
[25] T. D. Fridgen, X. K. Zhang, J. M. Parnis, R. E. March, *J. Phys. Chem. A* **2000**, *104*, 3487.
[26] a) J. T. Lyon, L. Andrews, *Inorg. Chem.* **2007**, *46*, 4799; b) J. T. Lyon, L. Andrews, *Organometallics* **2006**, *25*, 1341.
[27] B. O. Roos, R. Lindh, H.-G. Cho, L. Andrews, *J. Phys. Chem. A* **2007**, *111*, 6420.
[28] a) N. Ledoux, R. Drozdzak, B. Allaert, A. Linden, P. Van Der Voort, F. Verpoort, *Dalton Trans.* **2007**, 5201 (C=Ru bond length); b) P. Schwab, R. H. Grubbs, J. W. Ziller, *J. Am. Chem. Soc.* **1996**, *118*, 100 (C=Ru and C≡Ru bond lengths).
[29] D. L. Pavia, G. M. Lampman, S. K. George, *Introduction to Spectroscopy*, 3rd ed., Brooks Cole, New York, **2000**.
[30] A. E. Reed, L. A. Curtiss, F. Weinhold, *Chem. Rev.* **1988**, *88*, 899.
[31] G. Herzberg, *Infrared and Raman Spectra*, D. Van Nostrand, Princeton, NJ, **1945**.
[32] M. Zhou, L. Andrews, *J. Phys. Chem. A* **1999**, *103*, 6956.
[33] X. Wang, L. Andrews, unpublished data.
[34] Isotopic modifications synthesized: L. Andrews, H. Willner, F. T. Prochaska, *J. Fluorine Chem.* **1979**, *13*, 273.
[35] a) L. Andrews, A. Citra, *Chem. Rev.* **2002**, *102*, 885, and references cited therein; b) L. Andrews, *Chem. Soc. Rev.* **2004**, *33*, 123, and references cited therein.

Received: February 4, 2008
Published Online: April 18, 2007

